Short communication

# Upgraded photosensitivity under the influence of Yb doped on $V_2O_5$ thin films as an interfacial layer in MIS type Schottky barrier diode as photodiode application

V. Balasubramani [a], J. Chandrasekaran [a,*], V. Manikandan [b], Top Khac Le [c], R. Marnadu [a], P. Vivek [a]

[a] *Sri Ramakrishna Mission Vidyalaya College of Arts and Science, Coimbatore 641 020, Tamil Nadu, India*
[b] *Kongunadu Arts and Science College, Coimbatore 641 029, Tamil Nadu, India*
[c] *Department of Physics and Energy Harvest Storage Research Center, University of Ulsan, Ulsan 44610, Republic of Korea*

ARTICLE INFO

ABSTRACT

In this study, rare earth ytterbium (Yb)-doped $V_2O_5$ thin films were effectively coated on glass and Si substrates by the sol-gel method combined with the spin coating method. The films' structural, morphological, optical, and electrical properties were investigated through XRD, FESEM, UV-Vis, and I-V electrical conductivity. Doping on $V_2O_5$ with low Yb content of 2, 4, and 6 wt % have highly affected the lattice, which is shown in tetragonal and orthorhombic structures. Morphological studies show nanorods like structured. The coated thin films yield bandgap of 3.23–3.31 eV. The electrical properties of Cu/Yb@$V_2O_5$/n-Si type Schottky barrier diode were studied, and calculated photodiode parameters like photosensitivity, photo-responsivity, external quantum efficiency, and detectivity. Predominantly, high photosensitivity of 5545.70% is obtained for the diode with 2 wt % Yb@$V_2O_5$.

## 1. Introduction

Schottky diodes are the critical mechanisms of electronic and opto-electronic devices. Owing to their simple fabrication and multipurpose usage, they are used as potential components in solar cells, photodetectors, clamped transistors, metal-semiconductor field-effect transistor (MESFET), microwave mixers, radio frequency attenuators, rectifiers, varactors, Zener diodes, and several integrated circuits, etc., [1–5].

Schottky barrier diodes (SBDs) are often referred to as layered structures fabricated from metal-semiconductor (MS) and metal interfacial layer semiconductor (MIS) [6]. In contrast to the MS structure, the MIS structure's electrical properties may vary considerably due to the presence of the interfacial layer because the interfacial layer has a significant effect on the performance, stability, and reliability of the device. The thin interfacial layer acts as a dielectric medium that can prevent the inter-diffusion between MS junctions and levitate the electric field reduction issue in MS Schottky barrier diodes [1–7].

Among the various oxide phases from $V^{2+}$ to $V^{5+}$, $V_2O_5$ is thermodynamically most stable. $V_2O_5$ micro-nano structures have been widely used in the optical and electrochemical areas [8]. However, its electric

area applications have received less attention due to the low electrical conductivity at room temperature. Pure $V_2O_5$ is a semiconductor with a wide gap (Eg) of 3.3 eV, low carrier concentration (n) of $1015$-$10^{15} cm^{-3}$, and carrier mobility (μ) of 4.75–1.28 $cm^2 V^{-1} s^{-1}$ [9]. Therefore, the electrical conductivity of pure $V_2O_5$ is dependent on small polaron hopping (SPH), which leads to the low electrical conductivity of $10^{-2}$ to $10^0 \ \Omega^{-1} cm^{-1}$ [10]. Simulation and experimental results show that metal and rare earth elements doped-$V_2O_5$, composites based on $V_2O_5$, and novel morphologies of micro-nano structure alter the optical gap and improve the electrical conductivity of $V_2O_5$. Iida et al. [11] Investigated optical properties of the elements of $M_x V_{2-x} O_5$ (M = Nb, Ce, Nd, Dy, Sm, Ag, and Na). The results show that the optical gap increases with the Nb, Ce, Nd, Sm, and Dy while it decreases with the Ag and Na. The electrical conductivity of $M_x V_{2-x} O_5$ was also improved with M = Ag, Cu, Na, Mg, etc., [12–14].

Presently, rare earth (RE) materials gained lot of attention because they contribute significant modifications to structural and properties optical and create oxygen vacancies which is helpful for the electrical properties of SBDs device, Yb is the highest melting point among the RE materials, high dielectric constant, wide bandgap energy, low leakage

---

* Corresponding author.
  *E-mail address:* jchandaravind@yahoo.com (J. Chandrasekaran).
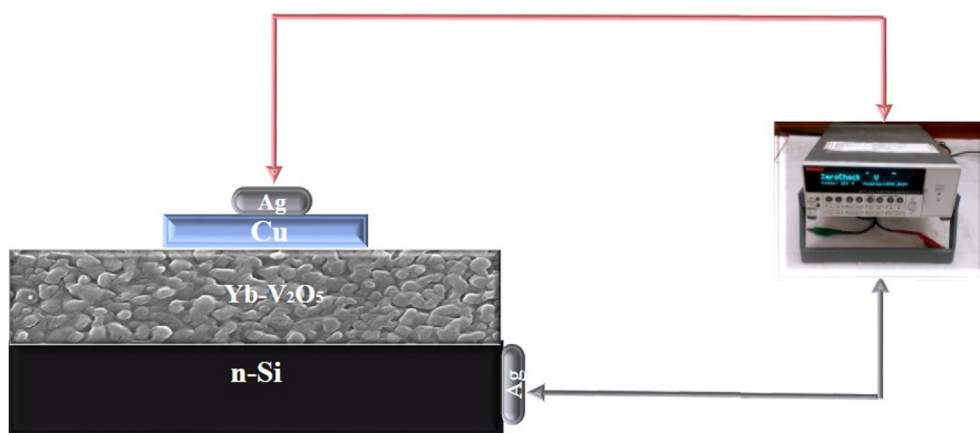
**Fig. 1.** Schematic diagram of Cu/Yb@$V_2O_5$/n-Si Schottky barrier diode.
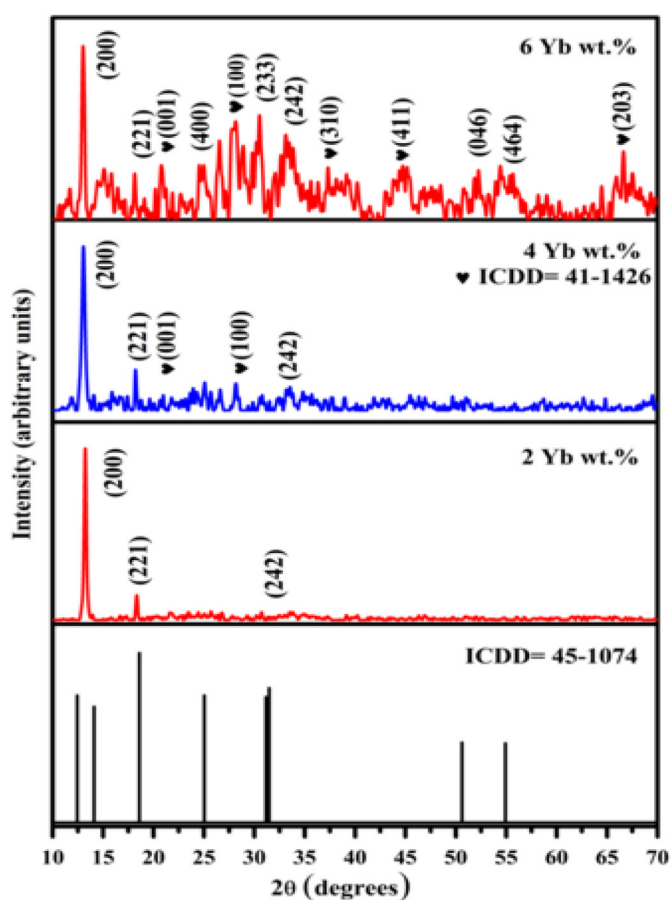


**Fig. 2.** Powder diffraction pattern of Yb@$V_2O_5$ thin films.



**Fig. 3.** XPS spectra of 6 wt% Yb@$V_2O_5$ film: a) survey spectrum, b) XPS spectrum of Yb 4 d

**Table 1**
Microstructural parameters of Yb@$V_2O_5$ films.

| Yb wt.% | Crystallite size (nm) ($D_{ave}$) | Dislocation density lines/m$^2$ ($\delta_{ave}$) | Micro strain ($\varepsilon_{ave}$) | Stacking fault x 10$^{-2}$ ($SF_{ave}$) |
|---|---|---|---|---|
| 0 | 42.07 | $1.26 \times 10^{15}$ | 1.229 | 0.1752 |
| 2 | 64.25 | $2.45 \times 10^{14}$ | 0.5425 | 0.8573 |
| 4 | 48.91 | $6.49 \times 10^{14}$ | 0.8170 | 0.2386 |
| 6 | 46.96 | $1.098 \times 10^{15}$ | 0.9900 | 0.3093 |

current, low-frequency dispersion, small hysteresis voltage, and broadly used in optical fiber [15–18]. Notably, the low work function of 2.63 eV can produce high Schottky barrier heights of diode [19]. The variation in atomic radii of Yb ions allows significant modifications of the crystalline structure, which affects the optical properties of those materials due to structural defects induced through the formation of the second phase
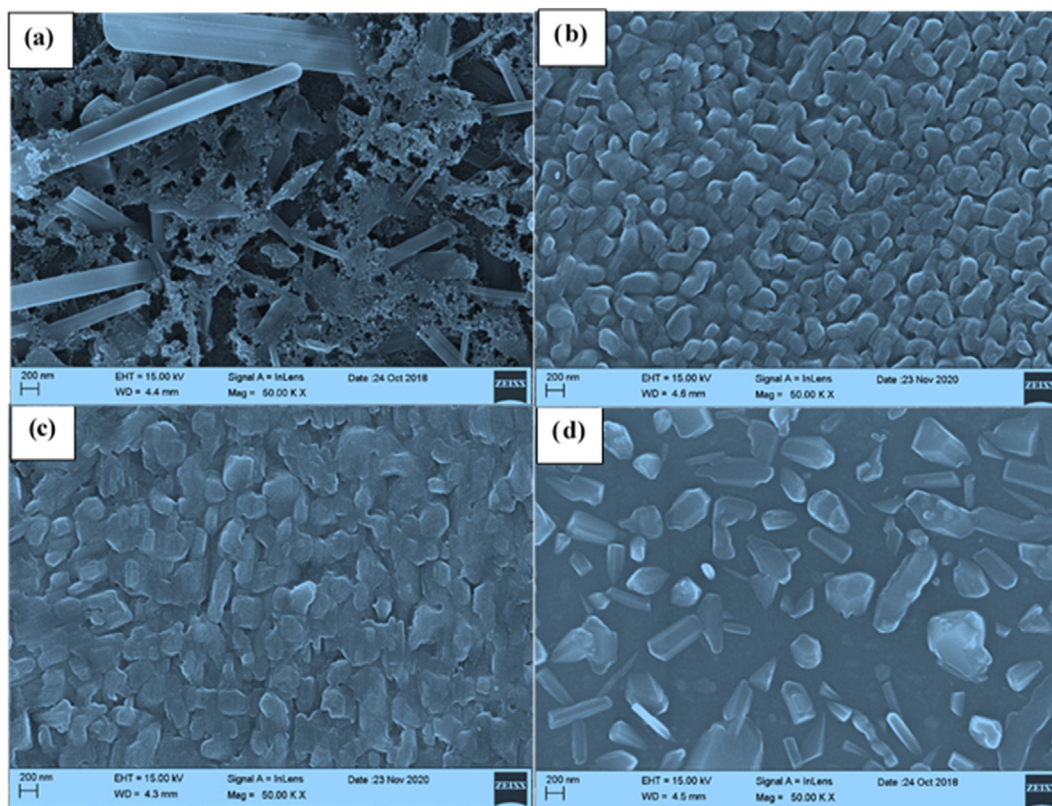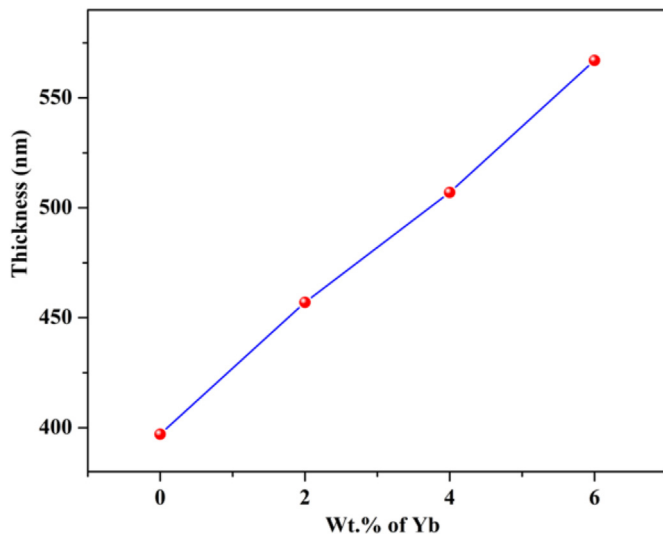
**Fig. 4.** FE-SEM Pictrure of Yb@$V_2O_5$ films.



**Fig. 5.** Thickness variation of Yb@$V_2O_5$ films.

within the host matrix of $V_2O_5$.

There are many coating techniques such as evaporation, sputtering, spin coating, spray pyrolysis. Moreover, jet nebulizer spray pyrolysis technique (JNSP) [20], pulsed laser deposition, chemical vapor deposition [21], solvothermal, electrodeposition [22–26], etc., sol-gel spin coating have been used for fabrication interfacial layer on MIS structured SBDs. Our device fabrication technique is an inexpensive, simple, and effective coating route because it controls surface morphology film, the stoichiometry of the film, crystal structure, and particle size by simply

changing growth parameters [23].

The objective of the present work is to prepare a high quality $V_2O_5$ thin films and incorporate Yb ions into the $V_2O_5$ matrix with various concentration such as 2, 4 and 6 wt%, by sol-gel spin coating technique. The prepared films were used as interfacial layer in between metal and semiconductor (MS) interface to develop the MIS Schottky barrier diodes. Also, the I–V performance of the MIS diode was evaluated under dark and light conditions. Various photo-diode parameters were calculated and discussed in detailed.

## 2. Experiment

### 2.1. Thin film coating procedure and fabrication of Schottky diode

The chemicals of vanadium chloride (VCl$_3$), ytterbium chloride hexahydrate (YbCl$_3$ · 6H$_2$O), and Triton as gelation agent (T100) were pick up during commencing Sigma Aldrich. A solvent is ethanol for all solutions. The primary pioneer solution was organized individually by vanadium chloride 0.2 M in 10 ml of the solution of ethanol, then stirred well via a magnetic stirrer for 1 hour. Triton X-100 chelating agent is added during stirrer. After that 2, 4, and 6 wt% ytterbium chloride were individually mixed into every solution and stirred aimed at 48 h s at room temperature. The prepared solution existed spin-coated proceeding the washed glass substrates at 2500 rpm used for 30 s. The films stayed annealing at elevated temperature of 500 °C intended for 1 hour as a final point. n-Si (100) type substrates were wrapped, winning a piranha solution for 20 min. Then, the etching acid for 15 min to get rid of the residual impurities on the substrates. The substrates were washed voguish deionized water and withered. Schottky's contact of Copper (Cu) coated on a surface of Yb@$V_2O_5$ layer via DC sputtering using high clarity Cu target. Finally, the silver paste (Ag) was used as an ohmic contact and painted on each side of the device. Fig. 1 shows the schematic diagram MIS type SBDs.
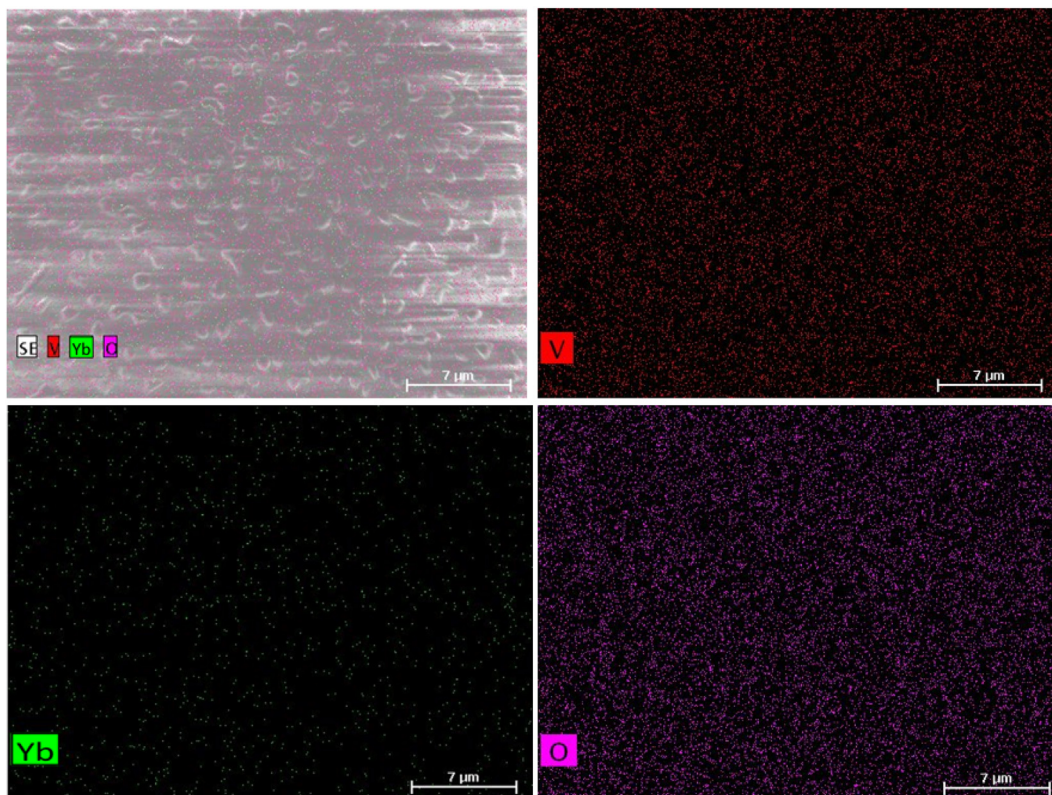
**Fig. 6.** EDX Mapping of 6 wt% Yb@V$_2$O$_5$ films.

**Table 2**
Atomic ratio pure and Yb@V$_2$O$_5$ films.

| Yb Wt % | Atomic ratio (%) | | |
|---|---|---|---|
| | V | O | Yb |
| **0** | 16.51 | 83.49 | - |
| **2** | 17.02 | 79.46 | 3.52 |
| **4** | 18.23 | 77.03 | 4.74 |
| **6** | 19.53 | 75.14 | 5.33 |

### 2.2. Characterization measurement

First, the quality of the prepared pure V$_2$O$_5$ and Yb@V$_2$O$_5$ thin films was analyzed by Rigaku Miniflex-II (CuKα, λ = 1.5418 Å) with the diffraction range of (10-80°). A stylus Profilometer detector (model: SJ-30) was used to measure the thickness of the film. Field emission scanning electron microscope (Zeiss Sigma model: FEI quanta 250) was used to analyze the surface and morphological behavior of Yb@V$_2$O$_5$ films. Elements like V, O, and Ce have been determined by energy dispersive X-ray analysis (EDX). The optical property was studied using UV-Vis Spectrometer (JASCO, model: V–770PC). Finally, the electrical properties of the prepared thin films have been determined using two probe instruments at different temperatures in the range of 30-150 °C. Keithley electro-meter (Model: 6517 B) was used to study the current Vs. Voltage (I–V) characteristics of the fabricated Cu/Yb@V$_2$O$_5$/n-Si diode. The photodiode property of the diode is analyzed by a portable solar simulator (PEC-L01) at 100 W/m$^2$ intensity.

### 3. Results and discussion

#### 3.1. XRD

Fig. 2 Displays X-ray diffraction patterns of Yb-doped V$_2$O$_5$ films,

display the occurrence of distinct peaks apportioned to (200) (221) and (242) planes of V$_2$O$_5$ tetragonal phase (ICDD card No. 45–1074). The higher Yb ions concentration affects the lattice periodicity of V$_2$O$_5$ and decreases the crystallization mentioned above process. The calculated crystallite size (D) of the Yb@V$_2$O$_5$ thin films was evaluated using the Scherrer equation [5];

$$D = \frac{k\lambda}{\beta \cos \theta} \tag{1}$$

Additionally, the lattice parameter Yb@V$_2$O$_5$ films existed planned via the resulting equation [5–7]:

$$\delta = \frac{1}{D^2} \tag{2}$$

$$\varepsilon = \beta \frac{\cos\theta}{4} \tag{3}$$

$$SF = \left[ \frac{2\pi^2}{45(3 \tan\theta)^{\frac{1}{2}}} \right] \beta \tag{4}$$

Table 1 demonstrates structural parameters of the combination of Yb keen on V$_2$O$_5$ crystallites. The reduction of the lattice parameter for Yb doped films come about with a sweeping reduction of the crystalline phase. This establishment plays an important role likely development of lonely Yb phases in the confines of V$_2$O$_5$ and may be influenced particle formation [27,28]. Remarkably, 2 wt% Yb@V$_2$O$_5$ film increase the defect on the surfaces of films and good crystallinity, which help enhance the density of active centers for high photo responsivity of the diode.

#### 3.2. XPS

For chemical composition analysis of Yb@V$_2$O$_5$ thin films, the XPS approach was applied. Fig. 3 indicates the XPS survey spectrum of
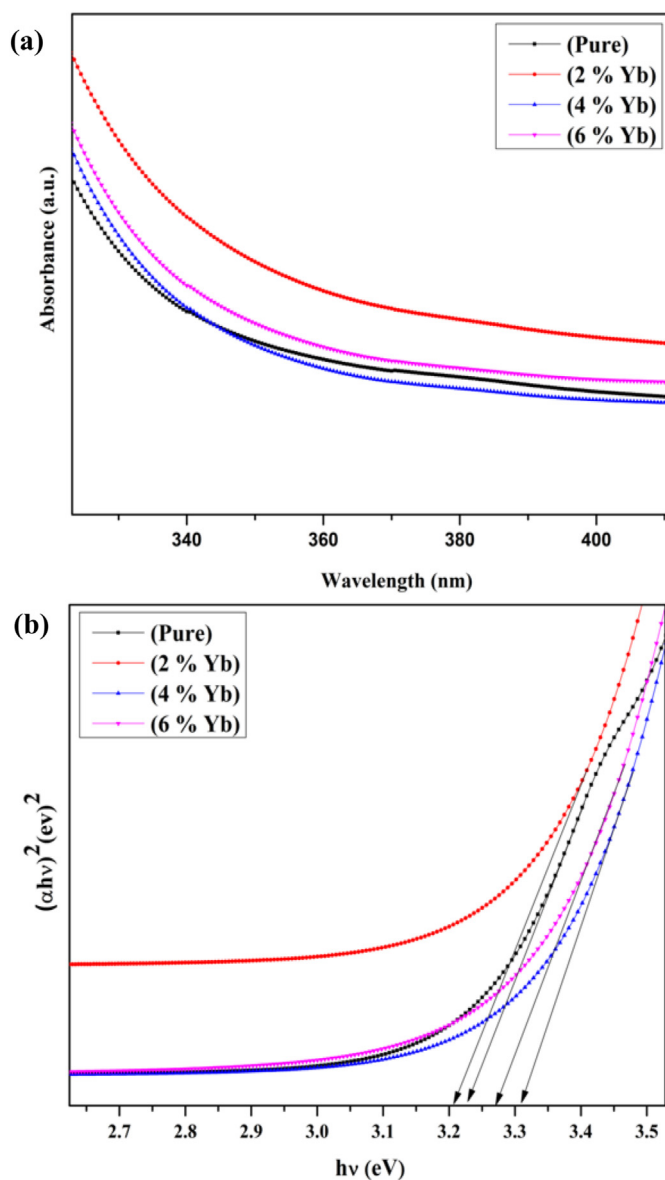
**(a)**

**(b)**

**Fig. 7.** Optical a) absorption b) band gap of pure and Yb@$V_2O_5$ films.

$Yb@V_2O_5$ thin film. The peaks corresponding to carbon (C), oxygen (O), vanadium (V), and (Yb) are certainly observed in the spectrum. A peak appeared at 281 eV in the XPS spectra is owing to the presence of carbon (C) which is owing to the hydrocarbon contamination on the surface of the thin film. The prominent peaks at different binding energies such as 496.6, 516.6, and 530 eV matching to V2p3/2, V2p1/2 and O1s, respectively. These binding energy values are according to the earlier stated data [29], which also supports the existence of $V^{5+}$ chemical form in the vanadium pentoxide thin film. Fig. 3b displays coupled peaks around 184.4 and 198 eV, which indicate the presence of Yb 4 d and are assigned respectively to 4 d 5/2 and 4 d 3/2 spin–orbit–split 4 d levels. These values are in good agreement with that of Yb 4 d level for $Yb^{+3}$ [30].

### 3.3. FE-SEM and EDX

Fig. 4 shows FE-SEM image pure $V_2O_5$ and Yb-doped $V_2O_5$ films. The undoped film shows nonuniform micro-nanorods with pours structured, as shown in Fig. 4a. The surface morphology of Yb@$V_2O_5$ strongly alters

and becomes a uniform rod-like array with the Yb doping concentrations, as shown Fig. 4 b-d. The rod-like structure and gran size of the $V_2O_5$ tend to increase as enhanced Yb concentration. With the further increase doping concentration of 6 wt%, the rod-likes have grown perpendicular to the substrate with void obelisk-shape. It is obvious from the surface morphology variations that the crystallite size has enriched. This surface alterations will boost the electrical properties of the $V_2O_5$ films FE-SEM of $V_2O_5$ films are loyal with XRD results. Evidently Yb with 2 wt % in $V_2O_5$ doped film will be appropriate interfacial layer for the device fabrication for optoelectronic applications. The thickness of the Yb@$V_2O_5$ films incresed from 397 to 567 nm on increasing the Yb wt.%, which is shown in Fig. 5. The results show that in the Yb played an active role on the thin layered films.

Fig. 6 Displays the EDX mapping of the 6 wt% of Yb-doped $V_2O_5$ thin film annealed at optimized temperature 500 °C. The EDX results exist composition of V, O, and Yb. The variation in atomic percentage for the Yb@$V_2O_5$ films was recorded in Table 2 as the minimum value of O was obtained at 2 wt% Yb@$V_2O_5$ films, which might be helpful in diode performance, to which convinced films can consume small electrical resistivity and owe to high conductivity as a result of oxygen deficiency [5–7].

### 3.4. UV-vis

Fig. 7a reveals absorption spectroscopy of Yb@$V_2O_5$ thin films with different Yb weight percentages. The absorption light slightly shifts toward a red light with Yb@$V_2O_5$. The intensity absorption of 2%Yb@$V_2O_5$ highest due to the highest densities of the rod-like arrays. The film's optical band gap has been calculated from Taue's plot and the flowing Eq (5) [4,8].

$$(\alpha h\nu)n = B(h\nu - Eg) \tag{5}$$

Where α is the absorption coefficient, hυ is the photon energy, and B is the constant.

The values of n = 2 for direct bandgap is evaluated, as shown in Fig. 7b, the optical gap of samples Yb = 0, 2, 4, and 6% are 3.23, 3.25, 3.31, and 3.27 eV, respectively. The doping of rare-earth ytterbium inside $V_2O_5$ can create defects that lead to the generation of excess electrons. These electrons can fill a part of the main CB and induce the wide optical gap with $E_{opt} = E_{opt0} + \Delta E_g^{BM}$, where $E_{opt0}$ is the optical gap of pure $V_2O_5$, and $\Delta E_g^{BM}$ is the Burstein-Moss shift [1]. Consequently, the optical gap of Yb-doped $V_2O_5$ increases compared with pure $V_2O_5$.

### 3.5. I–V dc electrical conductivity

Fig. 8 shows electrical characteristics of coated film using dc electrical studies. When temperature varied from range 30–150 °C, a linear increase current values of Yb@$V_2O_5$ films due to enormous heat energy absorbed by film and that induce the mobility of electrons [31–34]. This trend was similar to the voltage variation from 10 to 100 V. The resistivity of film varied from 1.21 to 5.80 × $10^{13}$Ω/cm with Yb doping concentration. Also, the average conductivity increase with doping concentration, higher conductivity, and minimum resistivity was obtained for Yb 2wt % films, which may be due to the presence of both tetragonal orthorhombic crystal structure formation and the swelling of grain size by way of dopant, which bargain the lattice dislocations and defectiveness of the V–O system. These spectacles decrease the grain boundary volume connected with the movement of charge carriers [34–39]. Mainly, the conductivity of the Yb@$V_2O_5$ films is thermally activated from the deep donor level to the conduction band, which tin can be related to the shrinking in the Nernst-Einstein movement and higher oxygen deficiency as confirmed in EDX results [40–42].

The dc electrical conductivity ($\sigma_{dc}$), activation energy films ($E_a$), and conductivity films ($\sigma_{dc}$) were calculated for pure and Yb@$V_2O_5$ thin films consuming the behind equation [6,7]:
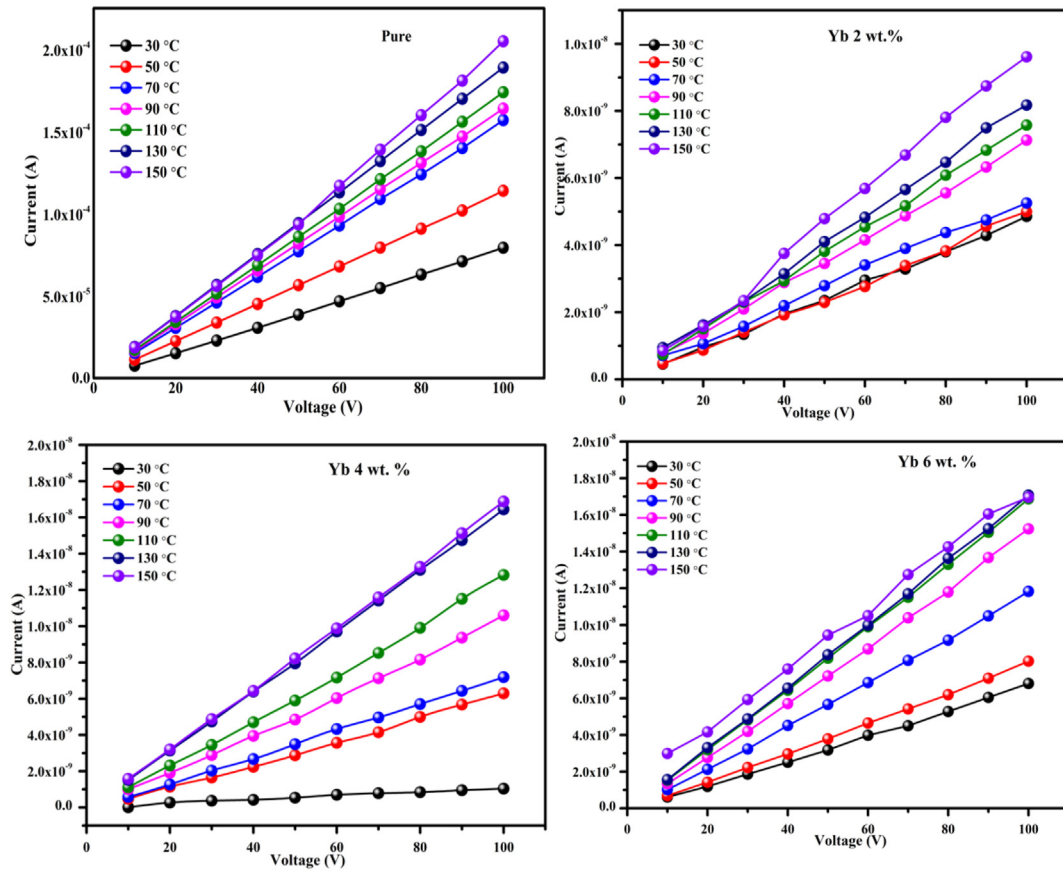
**Fig. 8.** I–V characteristics of pure $V_2O_5$ and Yb@$V_2O_5$ films.

$$\sigma = \left(\frac{t}{RA}\right)(\Omega\, cm)^{-1} \qquad (6)$$

$$\sigma = \sigma_0 \exp\left(\frac{-E_a}{K_B T}\right) \qquad (7)$$

The enhancement of jump distance between the vanadium ions and incorporation of Yb in $V_2O_5$ can reduce the segment of compact vanadium ion and lesser polaron populace [42–44].

### 3.6. Evaluation of Cu/Yb@$V_2O_5$/n-Si Schottky diode

The fabricated MIS type Schottky barrier diodes were forwarded, and reverse current values were measured by Keithley electrometer (6517-B) in the range of -4 V to 4. Fig. 9 Shows the I-V plot of pure andYb@$V_2O_5$ Schottky diodes. Based on the thermionic emission theory, the current conduction mechanism of the Cu/Yb@$V_2O_5$/n-Si diodes was explained using the following equation [1–7].

$$I = I_0[\exp(qv/nk_B T)] - 1 \qquad (8)$$

Thus barrier height ($\Phi_B$) and ideality factor (n) are calculated by following relation for all the diode in dark and light conditions [6].

$$n = \frac{q}{K_B T}\frac{dV}{d(\ln I)} \qquad (9)$$

$$\Delta_B = \frac{K_B}{q}\ln\left(\frac{AA^* T^2}{I_0}\right) \qquad (10)$$

The calculated n value change from 6.95 to 2.84 and these large values of n can be attributed to the high density of interface states localized at metal and semiconductor interface, and the effect of barrier

inhomogeneity, image force effect, recombination-generation, and tunneling might be possible mechanisms that can lead to an n value greater than unity [45–47]. Also, in a sufficiently thick interfacial layer, the interface states are in equilibrium with the inorganic semiconductor and cannot interact with the metal [48].

Fig. 10 displays the Semi-logarithmic forward and reverses bias ln (J) vs. V plot of pure and Yb@$V_2O_5$ MIS structured SBDs for dark and light conditions. It can be seen that ln (J) vs. V characteristics of the diode enhance with behavior of light condition. Current transport across inside diode is more effectively illumination-activated. The forward current at the high bias region increases slightly with increasing illumination intensity. This indicates slight light illumination production of electron-hole pair [49].

The calculated $\Phi_B$ value changes from 0.66 to 0.79 eV. It is seen that $\Phi_B$ depends on the changes in both illumination and voltage. This behavior shows that some trap charges have not enough energy to escape from the traps located between the metal and semiconductor interface in illumination [50–52]. The fabricated MIS structured SBDs shows a high photocurrent under light exhibits a significant photovoltaic effect [53].

The photodiode parameters such as photosensitivity (Ps), responsivity (R), Quantum efficiency (QE), and detectivity (D*) of the fabricated Cu/Yb@$V_2O_5$/n-Si MIS structure SBD's were calculated and listed in Table 3.

The photosensitivity can be calculated by the following equation [54]:

$$PS\% = \frac{I_{Ph} - I_D}{I_D} \times 100 \qquad (11)$$

Here, $I_D$ is the dark current of the diode, and $I_{ph}$-is the photocurrent of the diode. The calculated maximum photosensitivity of 5545.70% was obtained for 2 wt%. Yb@$V_2O_5$ diode. This huge photosensitivity shows
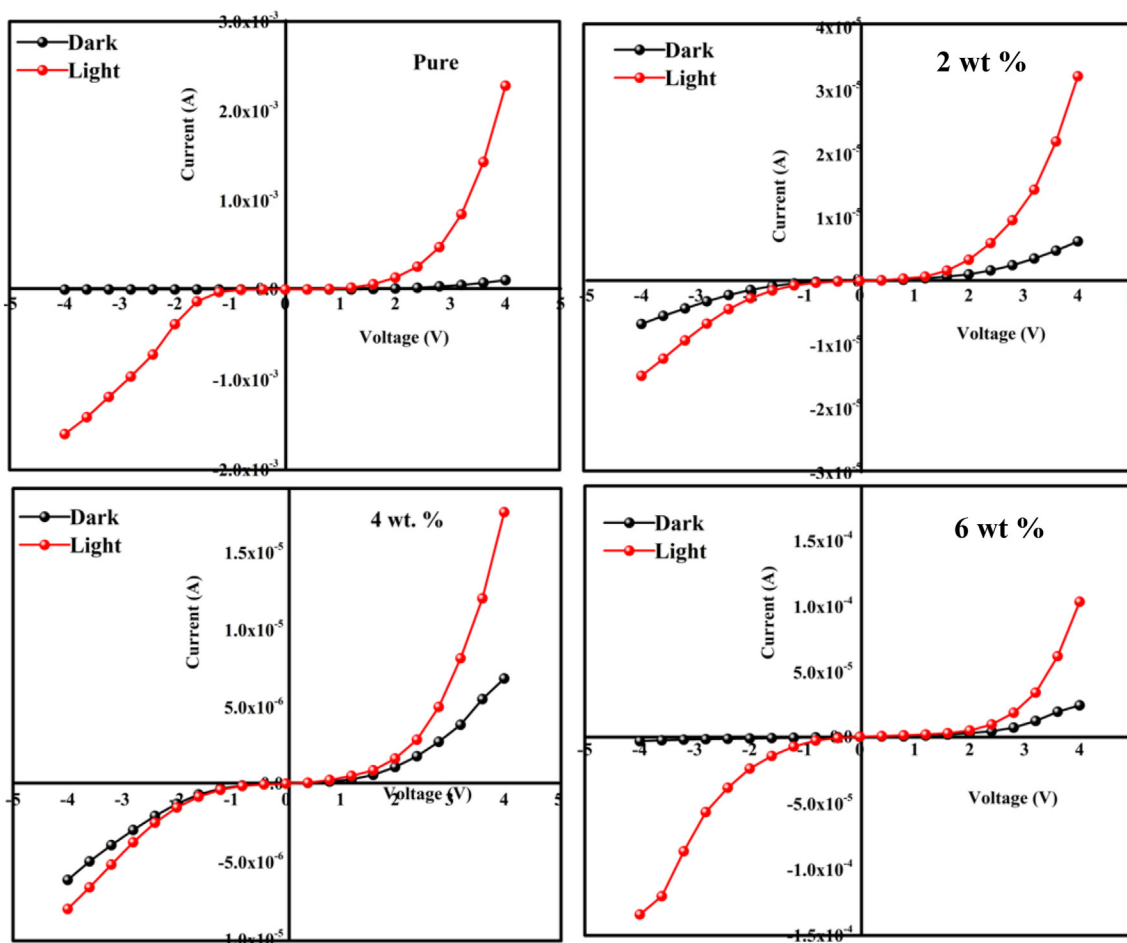
**Fig. 9.** IV plot of pure andYb@$V_2O_5$ Schottky barrier Diode.

that the incorporation of Yb content improved light absorption property [55]. The photo responsivity (R) is a critical parameter. It confirms the fraction of photocurrent and the light intensity of the active area of the diode, which can be calculated through the following equation [37].

$$R = \frac{I_{Ph}}{PA} \qquad (12)$$

Here, An area of the diode, $I_{ph}$ diode photocurrent value, and P light intensity. The obtained different values are 13.38–37.90 mA/W which is helpful for high-speed operation diode [56]. The maximum R-value was observed for 2 wt% of Yb@$V_2O_5$ diode due to photocurrent ratio to incident light intensity, indicating efficient Schottky photodiode responds to an optical signal [57]. The quantum efficiency is a vital photodiode parameter and contingent in the crystal structure, quality of diode, thickness of the interfacial layer, and internal resistance of the diode, is calculated using the following equation [38]:

$$QE = R\frac{hc}{q\lambda} \qquad (13)$$

Here, h Planck's constant value, c light velocity, q electron charge, λ wavelength. The obtained value of QE varied from 5.97 to 25.93%. The fabricated 2 Yb wt% photodiode compared with other diodes, high QE value estimated due to the QE are influenced by conversion rate from photons to electrons and holes [54,57]. The key parameter of application of photodetector is detectivity (D*), and it characterizes the weakest level of light intensity that constructs diode can detect, which is determined by responsivity and noise of the fabricated photodiode can be described by the following equation [39];

$$D^* = \frac{R}{(2qI_D)^{1/2}} \qquad (14)$$

Here, D* is the detectivity of the diode, R is the responsivity of the diode, $I_D$ is the dark current of the diode, and q is the electron charge. The D*values are increased from $8.87 \times 10^9$ to $9.97 \times 10^{10}$ Jones. The four noise sources often encountered in D* are values such as Johnson noise, shot noise 1/f noise, and photon noise [55–58]. Remarkably, 2 wt% of Yb@$V_2O_5$ diode detect high D* value $9.97 \times 10^{10}$ Jones, which incomes minimum noise extent in the sample. Based on the Cu/Yb@$V_2O_5$/n-Si MIS structure SBD's results, we saw that Yb content considerably modified the photodiode properties of the diode. These outcomes offer the low-cost fabrication of photodiode in photodetector application.

### 4. Conclusion

In summary, the Cu/Yb@$V_2O_5$/n-Si MIS structured SBDs diodes are successfully fabricated by the spin coating method. Doping $V_2O_5$ with Yb content 2, 4, and 6 wt % highly affected the lattice its tetragonal and orthorhombic structure present doped films. Morphological studies show nanorods and nanoplate-like structured observed. The coated thin films detected band gap varied from 3.23 to 3.31 eV. The electrical properties Cu/Yb@$V_2O_5$/n-Si type SBDs shows the photodiode performance under lighting condition is superior then dark, designating that fabricated diode performed like a photodiode. Remarkably, high photosensitivity of 5545.70% was obtained for the diode with 2 wt % Yb@$V_2O_5$ diode highly applicable candidate for the development of photodiode for optoelectronic application.
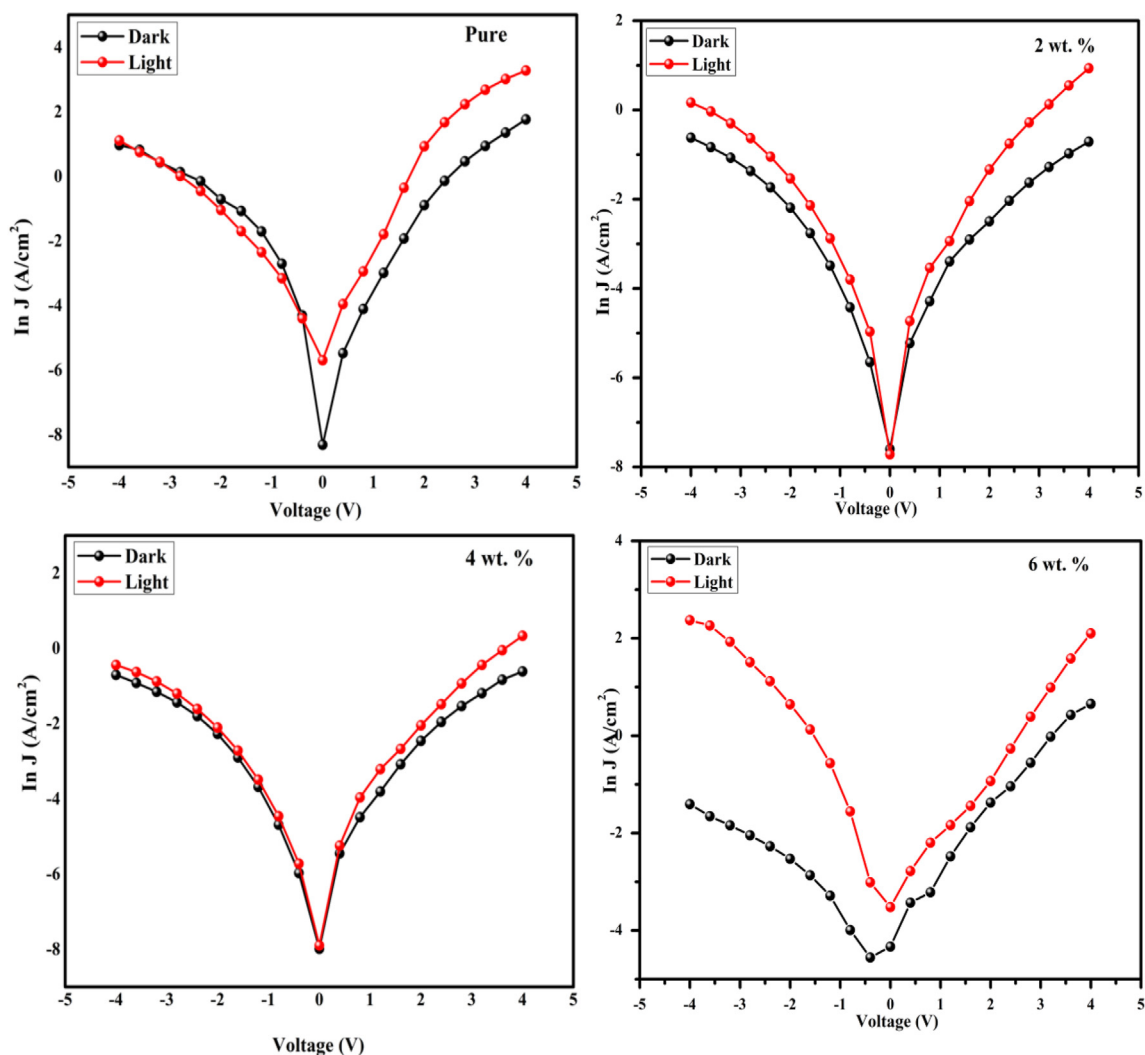
**Fig. 10.** Semi-logarithmic plot of In (J) vs V for Pure and Yb@$V_2O_5$ Schottky barrier diode.

**Table 3**
Photodiode parameters like n, $\Phi_B$, $I_0$, $P_s$, R, QE and D* are tabulated.

| Yb (wt.%) | n | | $\Phi_b$ (eV) | | Light condition | | | |
|---|---|---|---|---|---|---|---|---|
| | Dark | Light | Dark | Light | Photo-Sensitivity $P_s$ (%) | Responsivity R (mA/W) | Quantum efficiency QE (%) | Detectivity D* Jones |
| 0 | 6.95 | 5.09 | 0.66 | 0.67 | 748.82 | 13.38 | 5.97 | $8.87 \times 10^9$ |
| 2 | 2.48 | 2.03 | 0.89 | 0.93 | 75545.70 | 37.90 | 25.93 | $9.97 \times 10^{10}$ |
| 4 | 2.75 | 2.37 | 0.81 | 0.85 | 2225.50 | 29.79 | 20.85 | $9.43 \times 10^{10}$ |
| 6 | 3.24 | 2.84 | 0.75 | 0.79 | 961.90 | 23.53 | 17.90 | $9.13 \times 10^{10}$ |

## Author Statement

I herewith submit our revised manuscript entitled "Upgraded photosensitivity under the influence of Yb doped on $V_2O_5$ thin films as an interfacial layer in MIS type Schottky barrier diode as photodiode application" by V. Balasubramani, J. Chandrasekaran, V. Manikandan, Top khac le, R. Marnadu, P. Vivek. For your favourable consideration as a research paper in your esteemed journal "Journal of Solid State Chemistry" The manuscript is original and has been written by the stated authors, who are all aware of its content and have approved its submission. The article has not been published previously and is also not under consideration for publication elsewhere. There is no conflict of interests and, if accepted, the article will not be published elsewhere in the same form, in any language without the written consent of the publisher.

## Declaration of competing interest

The authors declare that they have no known competing financial interests or personal relationships that could have appeared to influence the work reported in this paper.

# References

[1] S. Mahato, D. Biswas, L.G. Gerling, C. Voz, J. Puigdollers, Analysis of temperature dependent current-voltage and capacitance-voltage characteristics of an Au/V$_2$O$_5$/n -Si Schottky diode, AIP Adv. 7 (2017), 085313, https://doi.org/10.1063/1.4993553.

[2] S. Mahato, J. Puigdollers, Temperature dependent current-voltage characteristics of Au/n -Si Schottky barrier diodes and the effect of transition metal oxides as an interface layer, Phys. B Phys. Condens. Matter. 530 (2018) 327–335, https://doi.org/10.1016/j.physb.2017.10.068.

[3] N.A. Al-Ahmadi, Metal oxide semiconductor-based Schottky diodes: a review of recent advances, Mater. Res. Express 7 (2020), https://doi.org/10.1088/2053-1591/ab7a60.

[4] P. Harishsenthil, J. Chandrasekaran, R. Marnadu, P. Balraju, C. Mahendarn, Influence of high dielectric HfO$_2$ thin films on the electrical properties of Al/HfO$_2$/n-Si (MIS) structured Schottky barrier diodes, Phys. B Condens. Matter 594 (2020) 412336, https://doi.org/10.1016/j.physb.2020.412336.

[5] V. Balasubramani, J. Chandrasekaran, T.D. Nguyen, S. Maruthamuthu, R. Marnadu, P. Vivek, S. Sugarthi, Colossal photosensitive boost in Schottky diode behaviour with Ce-V$_2$O$_5$ interfaced layer of MIS structure, Sensors Actuators, A Phys. 315 (2020) 112333, https://doi.org/10.1016/j.sna.2020.112333.

[6] V. Balasubramani, J. Chandrasekaran, V. Manikandan, R. Marnadu, P. Vivek, P. Balraju, Influence of rare earth doping concentrations on the properties of spin coated V$_2$O$_5$ thin films and Cu/Nd-V$_2$O$_5$/n-Si Schottky barrier diodes, Inorg. Chem. Commun. 119 (2020) 108072, https://doi.org/10.1016/j.inoche.2020.108072.

[7] V. Balasubramani, J. Chandrasekaran, R. Marnadu, P. Vivek, S. Maruthamuthu, S. Rajesh, Impact of annealing temperature on spin coated V2O5 thin films as interfacial layer in Cu/V$_2$O$_5$/n-Si structured Schottky barrier diodes, J. Inorg. Organomet. Polym. Mater. 29 (2019) 1533–1547, https://doi.org/10.1007/s10904-019-01117-z.

[8] T.K. Le, M. Kang, S.W. Kim, A review on the optical characterization of V$_2$O$_5$ micro-nanostructures Review article A review on the optical characterization of V$_2$ O$_5$ icro-nanostructures, Ceram. Int. 45 (2019) 15781–15798, https://doi.org/10.1016/j.ceramint.2019.05.339.

[9] M. Kang, J. Jung, S.Y. Lee, J.W. Ryu, S.W. Kim, Conductivity, carrier density, mobility, Seebeck coefficient, and power factor in V$_2$O$_5$, Thermochim. Acta 576 (2014) 71–74, https://doi.org/10.1016/j.tca.2013.11.026.

[10] S. Khan, K. Singh, Structural, optical, thermal and conducting properties of V$_2$−xLixO$_5$−δ (0.15 ≤ x ≤ 0.30) systems, Sci. Rep. 10 (2020) 1–11, https://doi.org/10.1038/s41598-020-57836-8.

[11] Y. Iida, Y. Kanno, Doping effect of M (M = Nb, Ce, Nd, Dy, Sm, Ag, and/or Na) on the growth of pulsed-laser deposited V$_2$O$_5$ thin films, J. Mater. Process. Technol. 209 (2009) 2421–2427, https://doi.org/10.1016/j.jmatprotec.2008.05.033.

[12] F. Coustier, S. Passerini, J. Hill, W.H. Smyrl, Silver-doped vanadium oxides as host materials for lithium intercalation, Mater. Res. Soc. Symp. Proc. 496 (1998) 353–358, https://doi.org/10.1557/proc-496-353.

[13] S. Iwanaga, M. Marciniak, R.B. Darling, F.S. Ohuchi, Thermopower and electrical conductivity of sodium-doped V$_2$O$_5$ thin films, J. Appl. Phys. 101 (2007), https://doi.org/10.1063/1.2739311.

[14] M. Panagopoulou, D. Vernardou, E. Koudoumas, N. Katsarakis, D. Tsoukalas, Y.S. Raptis, Tunable properties of Mg-doped V$_2$O$_5$ thin films for energy applications: Li-ion batteries and electrochromics, J. Phys. Chem. C 121 (2017) 70–79, https://doi.org/10.1021/acs.jpcc.6b09018.

[15] N. Puri, A. Rohilla, S.K. Chamoli, A.K. Mahapatro, Effect of ytterbium oxide deposition on microstructural and electrical properties of thin tantalum foil, Mater. Lett. 253 (2019) 67–70, https://doi.org/10.1016/j.matlet.2019.06.016.

[16] Y. Aktas, L. Arda, M. Acikgoz, Z.K. Heiba, S. Aktas, Preparation, growth, and magnetic properties of co-doped Yb$_2$O$_3$ Nanoparticles and thin films by the sol-gel process, J. Supercond. Nov. Magnetism 25 (2012) 2789–2793, https://doi.org/10.1007/s10948-011-1267-5.

[17] J. Zhou, F. Ye, L. Cheng, M. Li, W. Yue, Y. Wang, Microstructure and mechanical properties of Si$_3$ N4f/Si$_3$N$_4$ composites with different coatings, Ceram. Int. 45 (2019) 13308–13314, https://doi.org/10.1016/j.ceramint.2019.04.020.

[18] A. Prnová, K. Bodišová, R. Klement, M. Migát, P. Veteška, M. Škrátek, E. Bruneel, I. Van Driessche, D. Galusek, Preparation and characterization of Yb$_2$O$_3$-Al$_2$O$_3$ glasses by the Pechini sol-gel method combined with flame synthesis, Ceram. Int. 40 (2014) 6179–6184, https://doi.org/10.1016/j.ceramint.2013.11.071.

[19] A. Kahraman, H. Karacali, E. Yilmaz, Impact and origin of the oxide-interface traps in Al/Yb$_2$O$_3$/n-Si/Al on the electrical characteristics, J. Alloys Compd. 825 (2020) 154171, https://doi.org/10.1016/j.jallcom.2020.154171.

[20] S. Beke, A review of the growth of V2O5 films from 1885 to 2010, Thin Solid Films 519 (2011) 1761–1771, https://doi.org/10.1016/j.tsf.2010.11.001.

[21] K. Sasikumar, R. Bharathikannan, M. Raja, B. Mohanbabu, Fabrication and characterization of rare earth (Ce, Gd, and Y) doped ZrO$_2$ based metal-insulator-semiconductor (MIS) type Schottky barrier diodes, Superlattice. Microst. 139 (2020) 106424, https://doi.org/10.1016/j.spmi.2020.106424.

[22] K. Sasikumar, R. Bharathikannan, M. Raja, Effect of annealing temperature on structural and electrical properties of Al/ZrO2/p-Si MIS Schottky diodes, Siliconindia 1–7 (2018), https://doi.org/10.1007/s12633-018-9938-5.

[23] K. Sasikumar, R. Bharathikannan, J. Chandrasekaran, M. Raja, Effect of organic additives on the characteristics of Al/organic additive:ZrO2/p-Si metal–insulator-semiconductor (MIS) type Schottky barrier diodes, J. Inorg. Organomet. Polym. Mater. 30 (2020) 564–572, https://doi.org/10.1007/s10904-019-01216-x.

[24] M.Z. Pedram, M. Kazemeini, M. Fattahi, A. Amjadian, A physicochemical evaluation of modified HZSM-5 catalyst utilized for production of dimethyl ether from

[25] methanol, Petrol. Sci. Technol. 32 (2014) 904–911, https://doi.org/10.1080/10916466.2011.615366.

[25] F.B. Shareh, M. Kazemeini, M. Asadi, M. Fattahi, Metal promoted mordenite catalyst for methanol conversion into light olefins, Petrol. Sci. Technol. 32 (2014) 1349–1356, https://doi.org/10.1080/10916466.2012.656871.

[26] M. Fattahi, M. Kazemeini, F. Khorasheh, A.M. Rashidi, Vanadium pentoxide catalyst over carbon-based nanomaterials for the oxidative dehydrogenation of propane, Ind. Eng. Chem. Res. 52 (2013) 16128–16141, https://doi.org/10.1021/ie4007358.

[27] S. Zargouni, S. El Whibi, E. Tessarolo, M. Rigon, A. Martucci, H. Ezzaouia, Structural properties and defect related luminescence of Yb-doped NiO sol-gel thin films, Superlattice. Microst. 138 (2020) 106361, https://doi.org/10.1016/j.spmi.2019.106361.

[28] M. Balestrieri, G. Ferblantier, S. Colis, G. Schmerber, C. Ulhaq-Bouillet, D. Muller, A. Slaoui, A. Dinia, Structural and optical properties of Yb-doped ZnO films deposited by magnetron reactive sputtering for photon conversion, Sol. Energy Mater. Sol. Cells 117 (2013) 363–371, https://doi.org/10.1016/j.solmat.2013.06.032.

[29] G. Ravinder, C.J. Sreelatha, P. Chandar rao, P. Nagaraju, Y. Vijayakumar, T. Sreekanth, Gossamer-like V$_2$O$_5$ thin films for the detection of toxic volatile organic compounds, J. Sci. Res. 13 (2021) 347–359, https://doi.org/10.3329/jsr.v13i2.49333.

[30] Y. Hanifehpour, S.W. Joo, N. Hamnabard, J.H. Jung, The electrochemical performance and catalytic properties of Ytterbium substitution on Manganese oxide nanoparticles: BET study; preparation and characterization, J. Mater. Sci. Mater. Electron. 30 (2019) 18897–18909, https://doi.org/10.1007/s10854-019-02246-4.

[31] P. Vivek, J. Chandrasekaran, R. Marnadu, S. Maruthamuthu, V. Balasubramani, Incorporation of Ba$^{2+}$ ions on the properties of MoO$_3$ thin films and fabrication of positive photo-response Cu/Ba–MoO$_3$/p-Si structured diodes, Superlattice. Microst. 133 (2019) 106197, https://doi.org/10.1016/j.spmi.2019.106197.

[32] P. Vivek, J. Chandrasekaran, R. Marnadu, S. Maruthamuthu, V. Balasubramani, P. Balraju, Zirconia modified nanostructured MoO$_3$ thin films deposited by spray pyrolysis technique for Cu/MoO$_3$-ZrO$_2$/p-Si structured Schottky barrier diode application, Optik 199 (2019) 163351, https://doi.org/10.1016/j.ijleo.2019.163351.

[33] M.S. Raman, N.S. kumar, J. Chandrasekaran, R. Priya, P. Baraneedharan, M. Chavali, Thermal annealing effects on structural, optical and electrical properties of V$_2$O$_5$ nanorods for photodiode application, Optik 157 (2018) 410–420, https://doi.org/10.1016/j.ijleo.2017.11.030.

[34] M. Raja, J. Chandrasekaran, M. Balaji, B. Janarthanan, Impact of annealing treatment on structural and dc electrical properties of spin coated tungsten trioxide thin films for Si/WO$_3$/Ag junction diode, Mater. Sci. Semicond. Process. 56 (2016) 145–154, https://doi.org/10.1016/j.mssp.2016.08.007.

[35] M. Raj, C. Joseph, M. Subramanian, V. Perumalsamy, V. Elayappan, Superior photoresponse MIS Schottky barrier diodes with nanoporous:Sn-WO$_3$ films for ultraviolet photodetector application, New J. Chem. 44 (2020) 7708–7718, https://doi.org/10.1039/d0nj00101e.

[36] R. Marnadu, J. Chandrasekaran, M. Raja, M. Balaji, V. Balasubramani, Impact of Zr content on multiphase zirconium–tungsten oxide (Zr–WOx) films and its MIS structure of Cu/Zr–WOx/p-Si Schottky barrier diodes, J. Mater. Sci. Mater. Electron. 29 (2018) 2618–2627, https://doi.org/10.1007/s10854-017-8187-5.

[37] R. Marnadu, J. Chandrasekaran, P. Vivek, V. Balasubramani, S. Maruthamuthu, Impact of Phase Transformation in WO3 Thin Films at Higher Temperature and its Compelling Interfacial Role in Cu/WO3/p–Si Structured Schottky Barrier Diodes, Z. Phys. Chem. 234 (2020) 355–379, https://doi.org/10.1515/zpch-2018-1289.

[38] R. Marnadu, J. Chandrasekaran, S. Maruthamuthu, V. Balasubramani, P. Vivek, R. Suresh, Ultra-high photoresponse with superiorly sensitive metal-insulator-semiconductor (MIS) structured diodes for UV photodetector application, Appl. Surf. Sci. 480 (2019) 308–322, https://doi.org/10.1016/j.apsusc.2019.02.214.

[39] R. Marnadu, J. Chandrasekaran, M. Balaji, S. Maruthamuthu, P. Balraju, Influence of metal work function and incorporation of Sr atom on WO$_3$ thin films for MIS and MIM structured SBDs, Superlattice. Microst. 119 (2018) 134–149, https://doi.org/10.1016/j.spmi.2018.04.049.

[40] P.D. Raj, S. Gupta, M. Sridharan, Influence of the crystalline nature of growing surface on the properties of vanadium pentoxide thin films, Ceram. Int. 43 (2017) 9401–9407, https://doi.org/10.1016/j.ceramint.2017.04.110.

[41] N. Singh, A. Umar, N. Singh, H. Fouad, O.Y. Alothman, F.Z. Haque, Highly sensitive optical ammonia gas sensor based on Sn Doped V$_2$O$_5$ Nanoparticles, Mater. Res. Bull. 108 (2018) 266–274, https://doi.org/10.1016/j.materresbull.2018.09.008.

[42] B. Etemadi, J. Mazloom, F.E. Ghodsi, Phase transition and surface morphology effects on optical, electrical and lithiation/delithiation behavior of nanostructured Ce-doped V$_2$O$_5$ thin films, Mater. Sci. Semicond. Process. 61 (2017) 99–106, https://doi.org/10.1016/j.mssp.2016.12.035.

[43] M. Balaji, J. Chandrasekaran, M. Raja, Role of substrate temperature on MoO$_3$ thin films by the JNS pyrolysis technique for P-N junction diode application, Mater. Sci. Semicond. Process. 43 (2016) 104–113, https://doi.org/10.1016/j.mssp.2015.12.009.

[44] R. Marnadu, J. Chandrasekaran, S. Maruthamuthu, P. Vivek, V. Balasubramani, P. Balraju, Jet nebulizer sprayed WO$_3$-nanoplate Arrays for high-photoresponsivity based metal–insulator–semiconductor structured Schottky barrier diodes, J. Inorg. Organomet. Polym. Mater. 30 (2019) 731–748, https://doi.org/10.1007/s10904-019-01285-y.

[45] Altindal, T. Tunç, H. Tecimer, I. Yücedaǧ, Electrical and photovoltaic properties of Au/(Ni, Zn)-doped PVA/n-Si structures in dark and under 250 W illumination level, Mater. Sci. Semicond. Process. 28 (2014) 48–53, https://doi.org/10.1016/j.mssp.2014.05.007.

[46] H. Altuntaş, Ş. Altindal, H. Shtrikman, S. Özçelik, A detailed study of current-voltage characteristics in Au/SiO$_2$/n-GaAs in wide temperature range, Microelectron. Reliab. 49 (2009) 904–911, https://doi.org/10.1016/j.microrel.2009.06.003.

[47] I. Dökme, Ş. Altindal, On the intersecting behaviour of experimental forward bias current-voltage (I-V) characteristics of Al/SiO$_2$/p-Si (MIS) Schottky diodes at low temperatures, Semicond. Sci. Technol. 21 (2006) 1053–1058, https://doi.org/10.1088/0268-1242/21/8/012.

[48] A. Mrigal, M. Addou, M.E. El Jouad, S. Khannyra, Electrochemical performance of the V$_2$O$_5$ and VO$_2$ thin films synthesized by spray pyrolysis technique, J. Mater. Environ. Sci. 8 (2017) 3598–3605, https://doi.org/10.1007/s10800-010-0249-9.

[49] I. Jyothi, V. Janardhanam, J.H. Kim, H.J. Yun, J.C. Jeong, H. Hong, S.N. Lee, C.J. Choi, Electrical and structural properties of Au/Yb Schottky contact on p-type GaN as a function of the annealing temperature, J. Alloys Compd. 688 (2016) 875–881, https://doi.org/10.1016/j.jallcom.2016.07.292.

[50] N.M. Abd-Alghafour, N.M. Ahmed, Z. Hassan, Fabrication and characterization of V$_2$O$_5$ nanorods based metal–semiconductor–metal photodetector, Sensors Actuators, A Phys. 250 (2016) 250–257, https://doi.org/10.1016/j.sna.2016.09.001.

[51] N.M. Abd-Alghafour, N.M. Ahmed, Z. Hassan, D. Abubakar, M. Bououdina, Gdwdhurguy, Influence of annealing duration on the growth of V$_2$O$_5$ nanorods synthesized by spray pyrolysis technique, Surf. Rev. Lett. 23 (2016), https://doi.org/10.1142/S0218625X16500578.

[52] N.M. Abd-Alghafour, N.M. Ahmed, Z. Hassan, S.M. Mohammad, M. Bououdina, M.K.M. Ali, Characterization of V$_2$O$_5$ nanorods grown by spray pyrolysis technique, J. Mater. Sci. Mater. Electron. 27 (2016) 4613–4621, https://doi.org/10.1007/s10854-016-4338-3.

[53] A. Tataroğlu, Ş. Altindal, Study on the frequency dependence of electrical and dielectric characteristics of Au/SnO$_2$/n-Si (MIS) structures, Microelectron. Eng. 85 (2008) 1866–1871, https://doi.org/10.1016/j.mee.2008.05.025.

[54] A. Kathalingam, S. Valanarasu, T. Ahamad, S.M. Alshehri, H.S. Kim, Spray pressure variation effect on the properties of CdS thin films for photodetector applications, Ceram. Int. 47 (6) (2020) 7608–7616, https://doi.org/10.1016/j.ceramint.2020.11.100.

[55] H. Wang, D.H. Kim, Perovskite-based photodetectors: materials and devices, Chem. Soc. Rev. 46 (2017) 5204–5236, https://doi.org/10.1039/c6cs00896h.

[56] T. Ji, Q. Liu, R. Zou, Y. Zhang, L. Wang, L. Sang, M. Liao, J. Hu, Enhanced UV-visible light photodetectors with a TiO$_2$/Si heterojunction using band engineering, J. Mater. Chem. C. 5 (2017) 12848–12856, https://doi.org/10.1039/C7TC04811D.

[57] S. Halder, B. Pal, A. Dey, S. Sil, P. Das, A. Biswas, P.P. Ray, Effect of graphene on improved photosensitivity of MoS$_2$-graphene composite based Schottky diode, Mater. Res. Bull. 118 (2019), https://doi.org/10.1016/j.materresbull.2019.110507.

[58] E. Şenarslan, B. Güzeldir, M. Sağlam, Effects of surface passivation on capacitance-voltage and conductance-voltage characteristics of Al/p-type Si/Al and Al/V$_2$O$_5$/p-type Si/Al diodes, J. Phys. Chem. Solid. 146 (2020), https://doi.org/10.1016/j.jpcs.2020.109564.